

Resonant spectra of quadrupolar anions

K. Fosseuz,¹ Xingze Mao (毛兴泽),¹ W. Nazarewicz,^{2,3} N. Michel,^{1,4} W. R. Garrett,⁵ and M. Płoszajczak⁴

¹*NSCL/FRIB Laboratory, Michigan State University, East Lansing, Michigan 48824, USA*

²*Department of Physics and Astronomy and FRIB Laboratory,
Michigan State University, East Lansing, Michigan 48824, USA*

³*Institute of Theoretical Physics, Faculty of Physics, University of Warsaw, 02-093 Warsaw, Poland*

⁴*Grand Accélérateur National d'Ions Lourds (GANIL),*

CEA/DSM - CNRS/IN2P3, BP 55027, F-14076 Caen Cedex, France

⁵*Department of Physics and Astronomy, University of Tennessee, Knoxville, Tennessee 37996, USA*

(Dated: November 5, 2018)

In quadrupole-bound anions, an extra electron is attached at a sufficiently large quadrupole moment of a neutral molecule, which is lacking a permanent dipole moment. The nature of the bound states and low-lying resonances of such anions is of interest for understanding the threshold behavior of open quantum systems in general. In this work, we investigate the properties of quadrupolar anions as extreme halo systems, the formation of rotational bands, and the transition from a subcritical to supercritical electric quadrupole moment. We solve the electron-plus-molecule problem using a non-adiabatic coupled-channel formalism by employing the Berggren ensemble, which explicitly contains bound states, narrow resonances, and the scattering continuum. We demonstrate that binding energies and radii of quadrupolar anions strictly follow the scaling laws for two-body halo systems. Contrary to the case of dipolar anions, ground-state band of quadrupolar anions smoothly extend into the continuum, and many rotational bands could be identified above the detachment threshold. We study the evolution of a bound state of an anion as it dives into the continuum at a critical quadrupole moment and we show that the associated critical exponent is consistent with the second-order phase transition. Everything considered, quadrupolar anions represent a perfect laboratory for the studies of marginally bound open quantum systems.

I. INTRODUCTION

Multipolar anions form a unique class of molecular open quantum systems [1–4], whose properties arise from the competition between the short-ranged electrostatic multipolar potential, nonadiabatic coupling of electronic motion to molecular rotation, and a strong coupling to the one-electron continuum. They thus represent prototypical extreme halos [5–12], and laboratories for similar systems, such as deformed halo nuclei that are governed by short-ranged potentials, non-adiabatic rotation, and a strong coupling to the one- or two-nucleon continuum. Moreover, general studies of resonances reveal a plethora of phenomena present in open quantum systems, such as exceptional points [13, 14], superradiance [15], near-threshold clustering [16–19], and resonance trapping [20]. Consequently, unique characteristics of multipolar molecules in the landscape of open quantum systems call for detailed studies of their resonant spectra.

The striking case of dipolar anions has been extensively studied [1–4], using effective potentials methods [1, 21–28] as well as *ab initio* approaches [29–36]. In this case, the attractive potential $1/r^2$ is singular and thus can support an infinite number of bound states [37] for a dipole moment that is greater than a certain critical value. This raised a question whether dipole-bound anions could be a realization of a quantum anomaly [38]. However, when considering the rotational motion of the system, the answer to this question is negative [39–41].

The value of the critical moment μ_c required to bind an extra electron has been first determined [42] by Fermi

and Teller [43] for a point-dipole ($\mu_c = 1.625$ D) and then generalized to an extended dipole with an infinite moment of inertia [44]. However, high resolution electron photodetachment experiments [27, 45–49] suggested a greater critical moment, which appeared to be consistent with nonadiabatic calculations ($\mu_c \sim 2.5$ D) including the rotational degrees of freedom of the anion [24, 26, 28, 50–55]. In this case, dipolar anions support only few bound states and the value of μ_c depends on the moment of inertia.

Moreover, rotational states in dipolar anions were expected to be strongly affected by the shallowness of the molecular potential and the nonadiabatic coupling of the electronic and molecular rotational motions [27, 48, 55–58]. The strong coupling of the attached electron to the continuum [59–65] renders the picture even more complex, with the existence of low-energy sharp resonances [45, 66–71] in various systems, and the modification of the Wigner’s law [72–74] for the dipolar field [54, 75–77], first observed in hydrogen atoms [78, 79] and then extended to different power-law potentials [75, 76].

In a previous study, using a pseudopotential method and the Berggren expansion technique [80], we showed that in hydrogen cyanide anions HCN^- the competition between continuum effects and rotations leads to a transition from the subthreshold strong-coupling regime, where the external electron is in a spatially extended bound halo state that follows the rotational motion of the molecule, to the weak-coupling regime, where the electron and molecular motions are largely decoupled.

The quadrupolar anions case seems more straightforward. The potential $1/r^3$ is singular for any attractive

value of the quadrupole moment and its asymptotic solutions are known analytically for a finite moment of inertia of the molecule. However, it has been an experimental challenge to find systems where the excess electron is bound only due to the electric quadrupole moment [4, 81]. While the attachment of an electron by a pure quadrupolar field has been proposed theoretically already in 1979 [82] for beryllium oxide anions $(\text{BeO})_2^-$, the first experimental evidence of a quadrupole-bound anion has been obtained only in 2004 [83], for the trans-succinonitrile ($\text{NC}-\text{CH}_2-\text{CH}_2-\text{CN}$) molecule, whose gauche conformer is actually dipole-bound. Even octupole-bound anions have been reported experimentally [84] as early as in 2000. Recently, state-of-the-art ab initio calculations on several quadrupole-bound anion candidates [85, 86] concluded that the quadrupole binding is much weaker than dipole binding as the electron-molecule potential is not dominated by one component.

One of the reason is that the attractive $1/r^3$ potential can attach an electron in very localized states [22, 23], near the neutral polar molecule. It is thus difficult if not impossible in realistic conditions, to disentangle whether the electron's binding energy comes solely from the long-range quadrupolar field [87–89]. As a case in point, the $(\text{BeO})_2^-$ anion has a rhombic neutral form with a zero dipole-moment and a large quadrupole moment, and is quadrupole-bound in its ground state (g.s.) according to ab initio calculations [90], but a critical quadrupole moment cannot be defined as for dipolar anions.

A controversial example remains the carbon disulfide CS_2^- quadrupole-bound candidate. On the one hand, it can be argued that its quadrupole moment, $-2.67466 ea_0^2$, is insufficient to attach an electron [90], but, on the other hand, it has a simple linear geometry in its neutral form, and ab initio calculations [89] have shown that CS_2^- can exist in an excited linear configuration that is stable towards autodetachment by about 0.0012 Ry, an energy compatible with binding energies in polar anions. Experimentally, the situation is also difficult to interpret [91]. Indeed, Rydberg electron transfer data [92–96] show a characteristic sharp peak in the Rydberg effective principal number $n^* \sim 17$ dependence for the formation of CS_2^- that undergo electric-field-induced detachment. This is usually understood as a signature of dipole- or quadrupole-bound states [51, 97].

While CS_2^- has a positive electron affinity of ~ 0.05 Ry [89, 98, 99], it does not easily attach a free electron directly to form a long-lived anion due to rapid autodetachment [100], and a stabilization process is required for its formation [93]. Moreover, the g.s. of CS_2^- is bent [93, 94, 98, 101] with an angle of about 132° . The predicted linear excited state of CS_2^- thus appears as a “doorway state” to the g.s. [97, 102]. This is also suggested by the fact that the $n^* \sim 17$ energy is close to the bending vibrational energy of the CS_2^- g.s. [91, 93, 94]. Whether the linear excited state of CS_2^- is a pure quadrupole-bound state or not, cannot be answered using simple models. However, simple models allow to shed light on particular

aspects of problems, such as, for example, the role of the rotational motion in the critical binding of an electron on an electric dipole.

We propose to investigate general properties of linear quadrupole-bound and unbound anions, using an electron-plus-molecule model and by taking into account the particle continuum. In this picture, the linear core is represented as a triad of point charges [103, 104] separated by a distance s , with two possible configurations: oblate $(-q, 2q, -q)$ and prolate $(q, -2q, q)$ with $q > 0$. Considering the cylindrical symmetry along the molecule axis (z -axis), and according to the Buckingham convention [105], the quadrupole moment is given by $Q_{zz}^\pm = \pm 2qs^2$, where the sign of Q_{zz} is given by the sign of the extremal charges in the triads.

For this simple geometry of the system and in the adiabatic limit, i.e., for an infinite moment of inertia of the neutral molecule, it is possible to calculate very precisely the positive and negative critical electric quadrupole moments of the core required to attach an excess electron [106] in a $J^\pi = 0^+$ state. In Ref. [106], using the finite-scaling method [107] recently introduced in atomic physics [108–110], the critical quadrupole moments have been expressed as a function of the scaled parameter $q_s = qs$, so that $Q_{zz}^\pm = \pm 2q_s s$. The critical values for the scaled parameter have been found to be: $q_{s,c}^+ = 3.98251 (ea_0)$ and $q_{s,c}^- = 1.46970 (ea_0)$, for prolate and oblate critical quadrupole moments, respectively, and are consistent with numerical calculations [111]. The quality of these estimates comes from the analyticity of the scaling property of the critical quadrupole moments. For that reason, we shall refer to these results as analytical in the following, even if they were arrived at numerically.

This paper is organized as follows. The model Hamiltonian is presented in Sec. II, as well as the coupled channel formulation of the Schrödinger equation and the methods used to solve it. The results are discussed in Sec. III. We benchmark our numerical calculations by comparing them to the analytical values of the critical electric quadrupole moments. Thereafter follows the general discussion of quadrupolar anions as extreme halo systems, and we analyze the properties of the g.s. band in the continuum. Finally, we discuss resonant spectra, with an emphasis on quasi-degenerate states. We also study the evolution of resonant states with the electric quadrupole moment. The conclusion and outlook are contained in Sec. IV.

II. MODEL AND METHODS

A. Hamiltonian

The schematic description of quadrupolar anions, in terms of a neutral molecular core plus an attached electron, is partially justified by the scale separation between binding energies of valence electron of the neutral

molecule, and the energy attachment of the extra electron. However, microscopic studies have shown that for the quadrupolar potential the attached electron in the g.s. configuration is still rather close to the “core”. In this study, however, we are interested in the low-energy states of quadrupolar anions, and in particular their resonances. For these very extended states the scale separation argument applies well [112, 113].

The rotational degrees of freedom of the molecular core are included within the particle-plus-rotor model [114] in a non-adiabatic manner as described in Refs. [28, 58, 80]. Moreover, since the attached electron is assumed to be rather far from the core, the spin-orbit interaction is neglected. In this picture, the model Hamiltonian can be written as:

$$H = \frac{\mathbf{p}_e^2}{2m_e} + \frac{\mathbf{j}_r^2}{2I} + V \quad (1)$$

where \mathbf{p}_e is the linear momentum of the attached electron, m_e – its mass, and I is the moment of inertia of the molecule. The total angular momentum is thus $\mathbf{J} = \boldsymbol{\ell} + \mathbf{j}_r$, with $\boldsymbol{\ell}$ being the orbital angular momentum of the electron, and \mathbf{j}_r the molecular angular momentum. The pseudopotential V that describes the interaction between the core and the electron [115] is expressed through a multipole expansion:

$$V(r, \theta) = \sum_{\lambda} V_{\lambda}(r) P_{\lambda}(\cos \theta), \quad (2)$$

where the radial part $V_{\lambda}(r)$ is the electrostatic potential of a the linear charge distribution $(\pm q, \mp 2q, \pm q)$:

$$V_{\lambda}(r) = \frac{e}{4\pi\epsilon_0} \frac{Q^{\pm}}{s^2} \begin{cases} \frac{1}{r_{>}} - \frac{1}{r} & \text{for } \lambda = 0 \\ \left(\frac{r_{<}}{r_{>}}\right)^{\lambda} \frac{1}{r_{>}} & \text{for } \lambda = 2, 4, 6 \dots \end{cases} \quad (3)$$

with $r_{>} = \max(r, s)$ and $r_{<} = \min(r, s)$.

B. Coupled channel equations

The Schrödinger equation can be conveniently expressed in the coupled-channel (CC) formalism, where the total wave function for a given total angular momentum J^{π} can be written as:

$$\Psi^{J^{\pi}}(r) = \sum_c u_c^{J^{\pi}}(r) \Theta_c^{J^{\pi}}, \quad (4)$$

where the index c labels the channels (ℓ, j_r) , and $u_c^{J^{\pi}}(r)$ and $\Theta_c^{J^{\pi}}$ are the radial and angular channel wave functions, respectively. Since the Hamiltonian is rotationally invariant, the wave function is independent of the total angular momentum projection M_J .

The CC equations are obtained by inserting the ansatz (4) in the Schrödinger equation:

$$\begin{aligned} & \left[\frac{d^2}{dr^2} - \frac{\ell(\ell+1)}{r^2} - \frac{j_r(j_r+1)}{I} + E^{J^{\pi}} \right] u_c^{J^{\pi}}(r) \\ & = \sum_{c'} V_{cc'}^{J^{\pi}}(r) u_{c'}^{J^{\pi}}(r) \end{aligned} \quad (5)$$

where $V_{c,c'}^{J^{\pi}}$ is the channel-channel coupling potential [28].

C. Berggren expansion method

To solve the CC equations, we apply two methods. The first is the conventional Direct Integration Method (DIM), described in Ref. [28]. In DIM, one integrates the CC equations from a given starting energy. This method gives very precise results when considering a limited number of channels, and bound states or fairly narrow resonances. The second method is the Berggren Expansion Method (BEM), described in Refs. [28, 80], which may give results slightly less precise than the DIM, if the latter applies, but much better results for a large number of channels and for broad resonances. Moreover, since this technique is based on a diagonalization approach, it does not require any starting energy to converge and yields the full spectrum.

In the BEM, each channel wave function in Eq. (4) is expanded in a single particle (s.p.) basis, the so-called Berggren basis [116], originally developed for configuration-interaction calculations in nuclear physics [117]. The Berggren basis is a generalization of the Newton basis [118] in the complex plane; it explicitly contains bound states, decaying resonances, and scattering continuum. The construction of the Berggren basis for each partial wave c is done as follows. In the first step, the discrete resonant (Gamow) solutions $\phi_c(k_i)$ of a given spherical one-body generating potential are calculated assuming the outgoing boundary conditions. In the next step, the bound states (k_i imaginary) and decaying resonances ($k_i = \alpha_i - i\beta_i$, $\alpha_i, \beta_i > 0$) that are relevant for the description of a physical system are selected and surrounded by a contour \mathcal{L}_c^+ of complex-energy scattering states $\phi_c(k)$ to ensure the completeness.

The completeness relation for the resulting Berggren basis corresponding to a channel c is:

$$\sum_i |\phi_c(k_i)\rangle \langle \tilde{\phi}_c(k_i)| + \int_{\mathcal{L}_c^+} dk |\phi_c(k)\rangle \langle \tilde{\phi}_c(k)| = \hat{1} \quad (6)$$

where the contour \mathcal{L}_c^+ starts at zero, surrounds the selected resonances and extends to $k \rightarrow +\infty$. The tilde symbols indicate time-reversal. One may notice that there is some freedom when it comes to the choice of the Berggren basis: the form of the generating potential; the selection of the discrete resonant states entering the completeness relation; and the form of the contour \mathcal{L}_c^+ .

In the present study, the Berggren basis for each partial wave is generated using the diagonal elements $V_{cc}(r)$ of the channel-channel coupling potential; such a choice improves the convergence of calculations. Because of the Cauchy’s integral theorem, the precise form of the contour \mathcal{L}_c^+ is unimportant, provided that all the selected discrete states lie between the contour and the real axis in the momentum plane.

The normalization of bound states is standard, while for decaying resonant states this is accomplished by

means of the exterior complex scaling [119–121]. The scattering states are normalized to the Dirac delta. In practical applications, the integral along the contour \mathcal{L}_c^+ in Eq. (6) is discretized using the Gauss-Legendre quadrature, and the selected scattering states are renormalized by the quadrature weights. The normalization of discretized scattering states reduces in practice to the Kronecker delta normalization. In the calculations presented in this study, the shape of the contour has been defined through three segments: the first segment connecting the origin and the point $k_{\text{peak}} = k_r - ik_i$ with $k_r, k_i > 0$; the second segment connecting points k_{peak} and k_{middle} (real); and the third segment lying on the real axis between k_{middle} and k_{max} . The momentum cut-off k_{max} has to be sufficiently large to ensure the completeness of the Berggren basis.

Since the Berggren basis explicitly contains bound states, resonances and scattering states, it is ideally suited for the description of very diffuse systems, such as halos or Rydberg states, and also for unstable resonant states. While the DIM is of limited applicability when the initial energy required to ensure the convergence has to be chosen very close to the exact value, the BEM may also suffer from a related problem. Indeed, the discrete states entering the Berggren basis are obtained by integrating the Schrödinger equation with $V_{cc}(r)$, which is a process that requires a choice of starting energy. In many situations, harmonic oscillator expansion of the potential provides a starting point that is good enough to ensure the converge of the integration method, but for very weakly bound states or long-range potentials, this may fail. For that reason, a different approach, less sensitive to the initial conditions, has been proposed.

The idea is to use the fact that the quality of the integration method with respect to the starting energy, is deteriorating faster than convergence speed of the eigenvalue $E_f < 0$. Thus, for a potential $W(\eta)$ that has a bound state with $E \rightarrow -\infty$ when $\eta \rightarrow +\infty$, it is always possible to find a starting energy E_0 so that the integration $\mathcal{I}(E_0, \eta_0)$ will always converge for a sufficiently large value of $\eta_0 > 0$. Once such a point has been found, it is possible to make the integration to converge to the physical eigenenergy $E_f < 0$ at the physical value of $\eta_f > 0$ that defines the actual potential.

Indeed, the initial eigenenergy $E_0(\eta_0)$ can be used as a starting energy to obtain $E_1(\eta_1) = E_1(\eta_0 + \Delta\eta(E_0))$ with $\eta_0 > \eta_1 \geq \eta_f$. The same operation can be repeated using $E_1(\eta_1)$ as a starting energy to get $E_2(\eta_2) = E_2(\eta_0 + \Delta\eta(E_0) + \Delta\eta(E_1))$, with $\eta_1 > \eta_2 \geq \eta_f$. After $N + 1$ iterations, one gets:

$$\sum_{n=0}^N \Delta\eta(E_n) = \eta_f - \eta_0 \quad (7)$$

In order to minimize the number of iterations, the partition of $\eta_f - \eta_0$ can be chosen to exploit the sensitivity of the direct integration with respect to the starting energy, which is increasing as $E \rightarrow 0^-$. Thus the steps $\Delta\eta(E_n)$ must be decreasing as $E \rightarrow 0^-$, to both (i) preserve the

stability of the integration at each step and (ii) minimize the number of steps by considering bigger steps for larger values of $E < 0$.

To perform the partition of $\eta_f - \eta_0$, any series u_n with $u_N = 0$ and $u_n > u_{n+1}$, and which preserves the stability of the integration, would suffice. If by U_N one denotes the sum of u_n , then the steps are defined by:

$$\Delta Q(E_n) = (Q_f - Q_0) \frac{u_n}{U_N} \quad (8)$$

In our case, $u_n = 1/(n+1) - 1/(N+1)$ has provided a good compromise. Such an improved iterative procedure for bound states turned out to be helpful for evaluating the critical value of the parameter $\eta = Q_{zz,c}^{\pm}$ of the quadrupolar potential, as in this case extraordinary accuracy and stability are required.

D. Identification of resonances

In the Berggren basis, the Hamiltonian matrix becomes complex symmetric even if the Hamiltonian itself is Hermitian. This has a direct practical consequence, since the diagonalization of the Hamiltonian matrix gives a set of eigenstates that contain the resonant spectrum (bound states and resonances) embedded in the discretized complex-energy scattering continuum. Because we are interested in resonant states, an identification procedure has to be used to identify them.

In the absence of poles in the Berggren basis, the overlap method [122, 123] usually applied in nuclear physics, based on the assumption that continuum states play a perturbative role, cannot be applied. In this case, one may rely on another property of physical solutions. Indeed, resonant states given by the diagonalization in the full space are a priori independent of the precise form of the contour \mathcal{L}_c^+ . The contour-independence of resonant solutions has been used to identify dipolar anion resonances in Ref. [80]. In the present study, we also utilize this technique. To this end, we take two contours \mathcal{L}_0^+ and \mathcal{L}_1^+ , which differ by the imaginary part of k_{peak} and are discretized using the same number of points. While scattering solutions obtained with these contours are shifted along the imaginary axis, the resonant states are fairly insensitive as the precise shape of the contour does not impact decaying solutions. For the identification of very weakly bound states and low-lying resonances, that are only given as a superposition of complex-energy scattering states in the BEM, the method based on the concept of contour independence has been essential.

III. RESULTS

A. Critical quadrupole moments

In order to benchmark the DIM and BEM as applied to quadrupolar anions, our adiabatic-limit results are

compared with the analytical results of Ref. [106] for the critical electric quadrupole moment $Q_{zz,c}^{\pm} = \pm 2q_{s,c}^{\pm}s$. The internuclear distance s is fixed at $1.6a_0$ as in Ref. [115]; this value is close to the internuclear distance in CS_2^- ($s = 1.554a_0$ [124]). The corresponding critical quadrupole moments are thus $Q_{zz,c}^- = -2.35152ea_0^2$ and $Q_{zz,c}^+ = 6.372016ea_0^2$.

In the DIM, the parameter that controls the accuracy of calculations is the orbital angular momentum cutoff ℓ_{max} that determines the size of the channel basis. For $\ell_{\text{max}} = 12$, the DIM gives a critical oblate quadrupole moment of $Q_{zz,c}^- = -2.35162ea_0^2$. In the BEM, in addition to ℓ_{max} , the momentum cutoff k_{max} needs to be fixed. By taking a real contour discretized with 80 points, and $k_{\text{max}} = 12a_0^{-1}$, one obtains $Q_{zz,c}^- = -2.35164ea_0^2$. The critical oblate quadrupole moment can be approached closely with both methods, because it corresponds to a configuration of the attached electron that is well localized around the two positive charges at the center of the molecule. Thus, the electron is expected to be primarily in low- ℓ orbits. For the prolate quadrupole moment, the situation is different. Here, the attached electron, attracted by the extremal positive charges, is less bound and higher- ℓ partial waves are expected to play a more important role. Indeed, as shown on Fig. 1, the DIM and BEM results do not approach the analytical value as closely as for the oblate configuration. For $\ell_{\text{max}} = 14$ (and $k_{\text{max}} = 12a_0^{-1}$) we obtained $Q_{zz,c}^+ = 6.3980ea_0^2$ and $6.3984ea_0^2$ with the DIM and BEM, respectively. While the convergence of $Q_{zz,c}^+$ with ℓ_{max} (and k_{max}) is slower than for $Q_{zz,c}^-$, DIM and BEM results are fairly consistent for $\ell_{\text{max}} = 14$ and $k_{\text{max}} = 12a_0^{-1}$, and our results are in agreement with the DIM result of Ref. [115].

In realistic molecules, the effect of Pauli blocking at short distances [22, 23, 125] reduces the binding in the oblate configuration; hence, in general, it is the prolate configuration that is more likely to bind electrons. Thus, while the oblate configuration results are useful for benchmarking purpose, their physical interpretation should be dealt with caution.

B. Halo scaling properties

In quantum systems, the wave function may extend into the classically forbidden region to form the halo structure [6, 11] when the energy of a bound state approaches the threshold. The halo property can appear for many types of interactions [6]. In the case of two-body halo systems, the radial extension of the system, measured by the root-mean-square (r.m.s.) radius r_{rms}^2 changes with the separation (or detachment) energy E and ℓ according to the simple law [5]:

$$r_{\text{rms}}^2 \propto \begin{cases} |E|^{-1} & \text{for } \ell = 0, \\ |E|^{-\frac{1}{2}} & \text{for } \ell = 1, \end{cases} \quad (9)$$

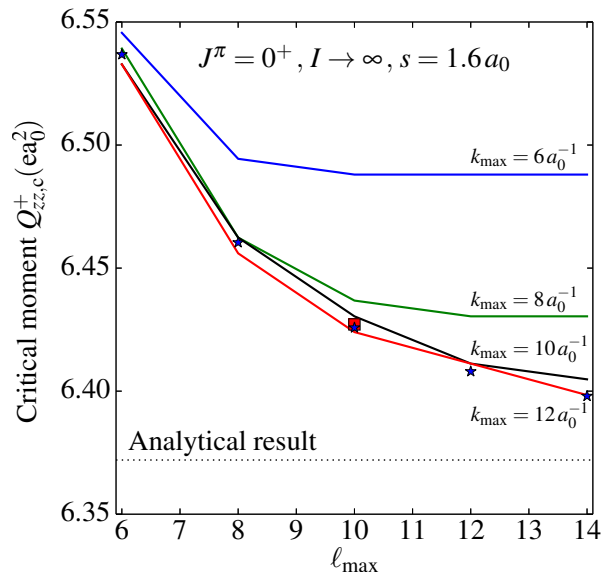


FIG. 1. Critical prolate electric quadrupole moment as a function of the orbital angular momentum cutoff in coupled-channel calculations in the adiabatic limit ($I \rightarrow \infty$). The internuclear distance is fixed at $s = 1.6a_0$ and the corresponding value of $Q_{zz,c}^+ = 6.372016ea_0^2$ is indicated by the dotted line. The DIM results are marked by stars. The DIM result from Ref. [115] is denoted by a square at $\ell_{\text{max}} = 10$. The convergence of the BEM results with respect to the momentum cutoff is shown for $k_{\text{max}} = 6, 8, 10$, and $12a_0^{-1}$.

while for higher angular momenta r_{rms}^2 stays finite when $|E| \rightarrow 0^-$. It should be remarked that deformation of the potential should not influence the halo properties [126, 127]. In principle, to compare two-body halo systems at various scales, the r.m.s. radius and the binding energy have to be rescaled for each potential considered. In the present work, no rescaling has been applied since we do not intend to compare different halo systems. Our goal to demonstrate that low-energy bound states in quadrupolar anions are behaving according to the laws expressed in Eq. (9).

Figure 2 shows r_{rms}^2 for the $J^\pi = 0^+$ and 2^+ states in both oblate and prolate configurations. The internuclear distance has been fixed at $s = 1.6a_0$ and the moment of inertia at $I = 10^4 m_e a_0^2$. The quadrupole moment has been adjusted for both configurations to give a bound state at around $E \sim -1.0 \cdot 10^{-2}$ Ry and then gradually changed to approach the critical value. All results have been obtained using the DIM and for an orbital angular momentum cutoff of $\ell_{\text{max}} = 8$. No bound states have been found for $J^\pi = 1^-$ and 3^- .

There is no difference in the scaling behavior for oblate and prolate configurations since in both cases the bound states are dominated by the same channels. The 0^+ states have $\ell = 0$ dominant channels and their r.m.s. radii scale according to Eq. (9). The 2^+ states are dominated by $\ell = 2$ partial waves; here, r_{rms}^2 reaches an asymptotic limit slightly below $1000a_0^2$.

For completeness, selected results for dipolar anions

are also shown in Fig. 2 to illustrate the similarity with quadrupolar systems. The results for the 0^+ g.s. of LiI^- , LiCl^- , LiF^- , and LiH^- [28] follow the $\ell = 0$ scaling, while the radii of 0^+ , 1^- , and 2^+ states in HCN^- [80] exhibit the $\ell = 1$ asymptotic behavior. For both dipolar and quadrupolar anions, the scaling laws (9) are satisfied extremely well, with r_{rms}^2 and $|E|$ spanning about five orders of magnitude. In this sense, polar anions should be viewed as extreme halo systems.

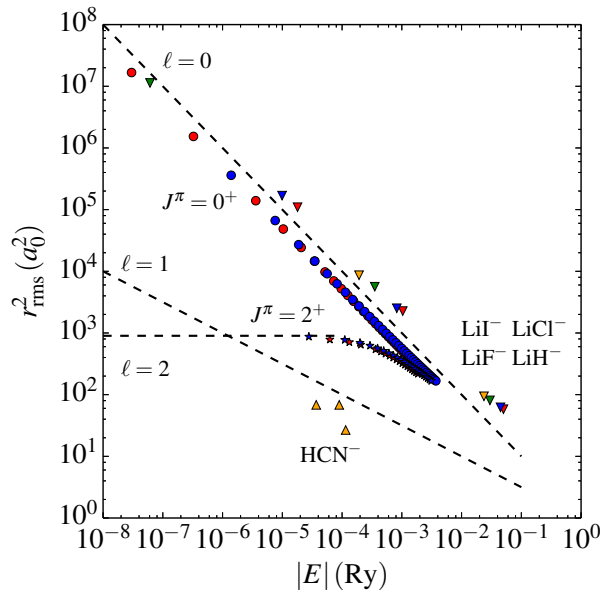


FIG. 2. Scaling plot $r_{\text{rms}}^2(|E|)$ for quadrupolar anions as two-body halo systems. Dashed lines represent the asymptotic behavior given by Eq. (9). The $\ell = 2$ line has been adjusted to the maximal r.m.s. radius of the $J^\pi = 2^+$ bound states. Results for $J^\pi = 0^+$ and 2^+ are marked with circles and stars, respectively. Oblate/prolate states are shown in red/blue. Selected results for dipolar anions [28, 80] are also indicated (triangles). Here, both $\ell = 0$ and $\ell = 1$ scaling laws are met.

C. Rotational bands in the continuum

In a previous BEM study on dipolar anions [80] it has been shown that the yrast band in HCN^- does not extend above the particle emission threshold. Namely, at the threshold, there appears a transition from the strong-coupling regime, in which the attached electron follows the rotational motion of the core, to the weak-coupling regime, where the electron's rotational motion is almost decoupled from that of the rotor.

Compared to the dipolar potential, the quadrupolar potential has a faster asymptotic falloff ($\propto 1/r^3$) that may affect the structure of delocalized resonant states. The impact on localized metastable states is less obvious. In order to answer this question, the binding energy for $Q_{zz}^- = -2.42 ea_0^2$ and $Q_{zz}^+ = +6.88 ea_0^2$ is plotted in Figs. 3(a) and 3(b), respectively, as a function of $J(J+1)$.

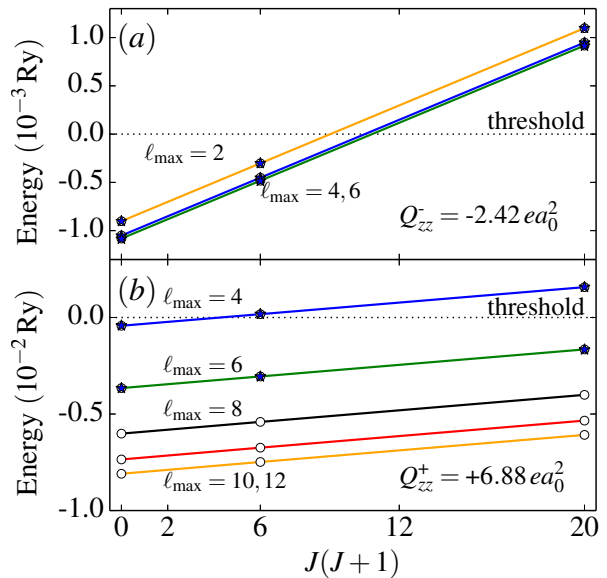


FIG. 3. Yrast band $K_J = 0$ of quadrupolar anions defined by an internuclear distance of $s = 1.6 a_0$, a moment of inertia of $I = 10^4 m_e a_0^2$, and quadrupole moments of $Q_{zz}^- = -2.42 ea_0^2$ and $Q_{zz}^+ = +6.88 ea_0^2$ on panels (a) and (b), respectively. The BEM and DIM results are denoted with empty circles and stars, respectively, and are almost indistinguishable for all orbital angular momentum cutoffs considered.

Here we use the same parameters as in the previous section ($s = 1.6 a_0$ and $I = 10^4 m_e a_0^2$). The contour \mathcal{L}_c^+ is identical for all partial waves. It starts at zero and is defined by the three points: $(0.3, -10^{-5})$, $(0.6, 0)$, and $(6, 0)$ (all in a_0^{-1}). The three resulting segments are discretized with 30, 30, and 40 scattering states, respectively. The specific values of Q_{zz} have been chosen so that the binding energy goes to zero for a total angular momentum $J \approx 2, 3$ at $\ell_{\text{max}} = 4$.

The BEM and DIM results are practically indistinguishable for all the values of ℓ_{max} considered. A perfect rotational behavior is predicted for both prolate and oblate configurations, even above the detachment threshold. This is confirmed by the collapse of all eigenenergies to the same bandhead energy in the adiabatic limit ($I \rightarrow \infty$). At the maximal orbital angular momentum cutoff ℓ_{max} considered, the states in the lowest-energy (yrast) band are all dominated by the $\ell = 0$ channel at about 99.7% and 87.9%, for the oblate and prolate configuration, respectively. Unlike in the dipolar case, rotational bands of quadrupolar anions persist in the continuum. The widths of unbound band members are very small ($\Gamma \sim 10^{-10}$ Ry).

In the intrinsic frame of the molecule, only the $K_J = 0$ component of the attached electron's density remains nonzero. Consequently, the densities $\rho_{J,K_J}(\mathbf{r})$ with $K_J = 0$ can be called intrinsic densities [80]. Figure 4 show the intrinsic densities for the $J^\pi = 0^+$, 2^+ , and 4^+ members of oblate and prolate bands. One can see that $\rho_{J,0}$ are practically identical within each band.

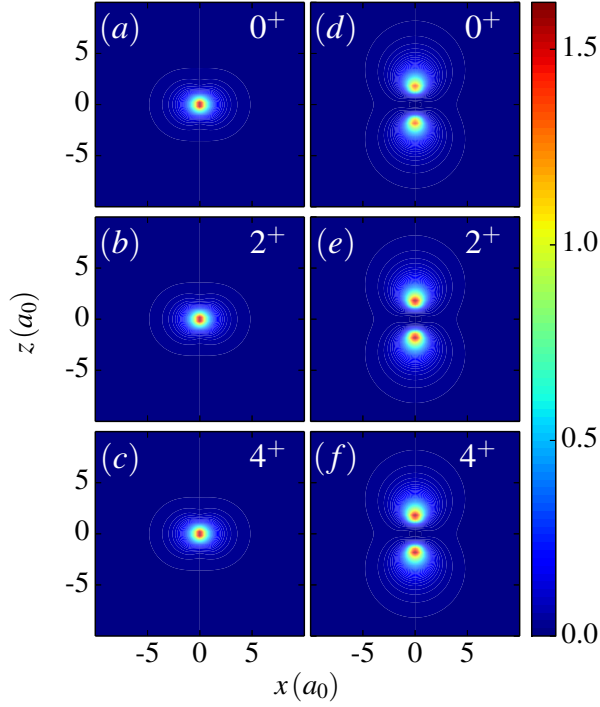


FIG. 4. Intrinsic densities $\rho_{J,0}(r)$ (in $10^{-2} a_0^{-3}$) for the yrast bands of Fig. 3 calculated with $\ell_{\max} = 6$. The densities for $J^\pi = 0^+$, 2^+ , and 4^+ are shown for both oblate (a-c) and prolate (d-f) configurations.

D. Resonances

The analysis of the unbound spectrum in quadrupolar anions can be conveniently performed using the BEM. Indeed, with the BEM one obtains the full spectrum in one diagonalization; calculations stay tractable with the increased number of channels; and the method does not require precise initial eigenvalues as in the DIM case.

Resonant spectrum calculations have been performed for the $J^\pi = 0^+$, 1^- and 2^+ states in oblate and prolate configurations ($Q_{zz}^- = -2.42 ea_0^2$, $Q_{zz}^+ = +6.88 ea_0^2$) for $\ell_{\max} = 8$, $s = 1.6 a_0$, and $I = 10^4 m_e a_0^2$. The contour \mathcal{L}_c^+ for each partial wave starts at zero and is defined by the three points: $(0.3, -10^{-5})$, $(0.6, 0)$, and $(12, 0)$ (all in a_0^{-1}). The resulting segments have been discretized with 60, 40 and 100 points representing scattering states.

Calculations reveal the presence of families of narrow decaying resonances in the complex-energy plane as shown in Figs. 5 and 6 for oblate and prolate configurations, respectively. The resonant structures are remarkably similar for oblate and prolate configurations, with widths ranging from 10^{-10} Ry to 10^{-6} Ry corresponding to lifetimes in the range of $10^{-7} - 10^{-11}$ s.

Each family of resonances, marked by the same symbol and color in Figs. 5 and 6, is characterized by one dominant channel (ℓ, j_r) that represent about 99% of the total wave function, except for those indicated by empty symbols. Within each family, narrow resonances have a

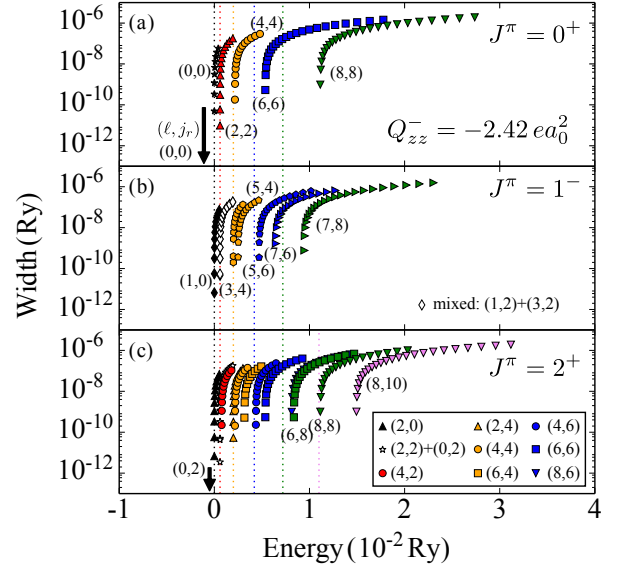


FIG. 5. The distribution of $J^\pi = 0^+$, 1^- , and 2^+ resonant states in the complex energy plane for the oblate configuration with $Q_{zz}^- = -2.42 ea_0^2$, $s = 1.6 a_0$, and $I = 10^4 m_e a_0^2$ calculated with $\ell_{\max} = 8$. Bound states are marked by arrows. In most cases, families of resonances are characterized by one dominant channel; the corresponding labels (ℓ, j_r) are given. Mixed groups are represented by empty symbols. Dashed lines indicate rotational energies of the molecule, $E_{j_r} = \hbar^2 j_r(j_r + 1)/(2I)$.

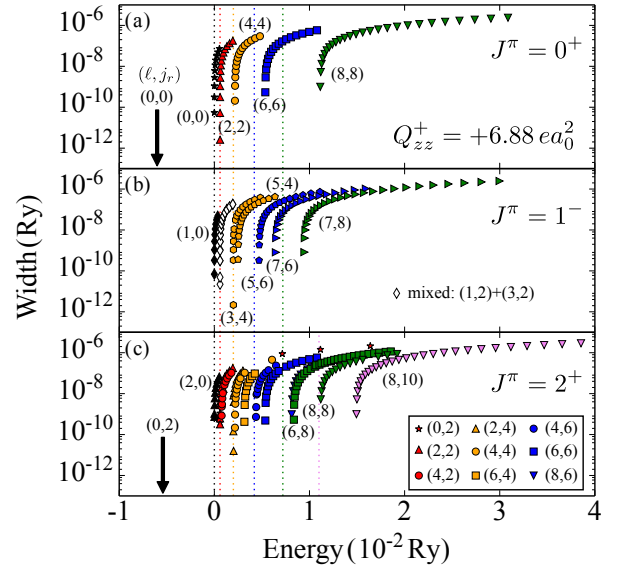


FIG. 6. Similar as in Fig. 5 but for a prolate configuration with $Q_{zz}^+ = +6.88 ea_0^2$.

very diffuse dominant-channel wave function with a small number of nodes, while broader resonances tend to have wave functions peaked closer to the origin and having larger numbers of nodes. Overall, energies of resonances tend to cluster close to the rotational states of the core, except for higher excitations where significant deviations

can be seen. Indeed, higher-lying resonances have larger values of the orbital angular momentum ℓ in their dominant channel, which results in larger centrifugal barriers.

The similarity of resonant structures predicted for oblate and prolate configurations at different J^π states can be explained in terms of the large delocalization of wave functions over thousands of a_0 . Indeed, above the particle emission threshold, even high- ℓ states have the first peak of their wave function at few hundreds of a_0 . These resonances are consequently weakly sensitive to short-range details of the potential, and are mainly influenced by the asymptotic tail $\propto 1/r^3$ of the quadrupolar field. Moreover, rather small resonance widths, even for states dominated by an $\ell = 0$ channel, seem to be characteristic of multipolar potentials since the same prediction has been made for the HCN^- dipolar anion [80].

The pattern of families shown in Figs. 5 and 6 can be easily understood by considering angular momentum coupling. Namely, since for $J^\pi = 0^+$ states $\ell = j_r$, each family of resonances represents an electron perfectly antialigned with respect to the rotor’s angular momentum, and the steadily increasing energy distance between groups is due to the centrifugal barrier that grows with ℓ . The states within each family can be distinguished by their radial behavior, i.e., the number of nodes in the radial wave function.

For $J^\pi = 1^-$, the angular momentum selection rule becomes: $\ell = 1$ for $j_r = 0$ and $\ell = j_r \pm 1$ for $j_r = 2, 4, \dots$. This yields 8 families (note that since $\ell_{\text{max}} = 8$, there is only one channel with $j_r = 8$). As discussed below, the two families with $j_r = 2$ and $\ell = 1, 3$, marked by open symbols in Figs. 5 and 6, are practically degenerate. This explains the multiplicity of families for $J^\pi = 1^-$, and – in a similar way – for $J^\pi = 2^+$.

Because many resonances belonging to low- ℓ channels cluster around the rotational states of the molecule, the density of resonances in the complex energy plane is high, and accidental (near-)degeneracies occur. This results in a strong configuration mixing. Such families of resonances have two dominant channel wave functions at low energy, and are referred to as “mixed” groups in the following. In Figs. 5 and 6, mixed groups are the (1,2) and (3,2) families for $J^\pi = 1^-$ and the (0,2) and (2,2) families for $J^\pi = 2^+$.

Within each of these groups, there appear pairs of resonances, or “doublets”, with very close complex energies. To illustrate the strong mixing between overlapping resonances, in Fig. 7 we show the wave functions of six $J^\pi = 1^-$ doublets, belonging to the mixed group at the prolate configuration of Fig. 6(b). Their dominant channel wave functions are ($\ell = 1, j_r = 2$) and ($\ell = 3, j_r = 2$). For the lowest-energy doublets in a mixed group the channel mixing is maximal: the channel wave functions are almost identical and the total wave functions can be represented by their symmetric and asymmetric combinations, as in a textbook case of a two-state mixing. However, as the excitation energy increases, the doublets move apart slightly in the complex energy plane

and the channel wave functions start to differ. However, the configuration mixing still remains strong. Moreover, as one can see in Fig. 7, while the intrinsic densities for $K_J = 0$ and 1 are very different within a given doublet, they show similar structures for states within the same mixed group. At low energies, the $K_J = 0$ term dominates (with a weight of 71%) in each doublet and then its weight increases to about 74% for one state and decreases to about 68% for the other state of the doublet.

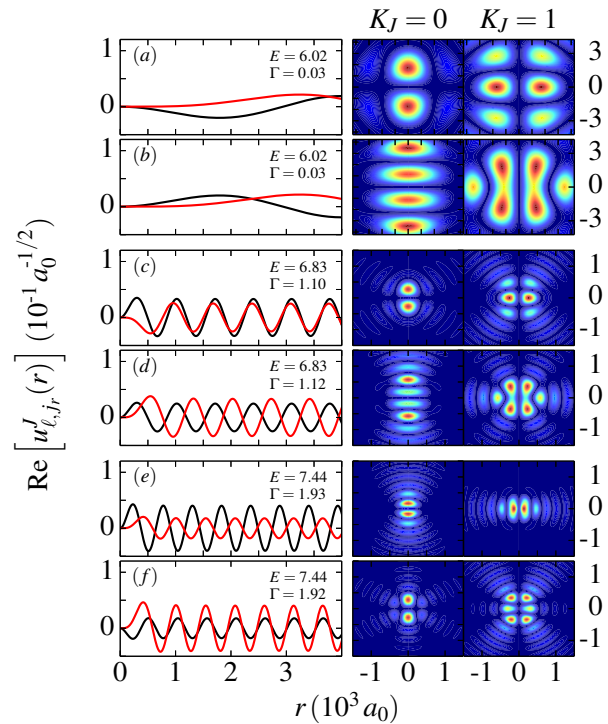


FIG. 7. Left: Real parts of the two dominant channel wave functions of selected quasi-degenerate $J^\pi = 1^-$ resonances of Fig. 6(b). The imaginary parts of the channel wave functions are about four orders of magnitude smaller. Resonance energies (in 10^{-4} Ry) and widths (in 10^{-8} Ry) are indicated. The channel wave functions (1,2) and (3,2) are colored black and red, respectively. Right: Corresponding intrinsic densities (in arbitrary units) for $K_J = 0$ and 1.

E. Evolution of the spectrum with the quadrupole moment

As demonstrated above, for the supercritical quadrupolar molecules with $|Q_{zz}^\pm| > |Q_{zz,c}^\pm|$, many resonances can exist in vicinity of the rotor energies. The subcritical quadrupolar molecules with $|Q_{zz}^\pm| < |Q_{zz,c}^\pm|$ may still accommodate resonances in spite of their weaker quadrupolar field.

The transition from a supercritical to subcritical quadrupolar anion is illustrated in Fig. 8 for $J^\pi = 0^+$ states. Figure 8(a) shows real energies of the lowest resonant states as a function of the quadrupole mo-

ment in an oblate system. If one denotes the energy of the i -th resonance of a supercritical molecule outside the critical region as E_i , then by changing the electric quadrupole moment continuously beyond $Q_{zz,c}^-$, one arrives at $E_i \rightarrow E'_i \approx E_{i+1}$. A close look at the area in the immediate vicinity of the critical quadrupole moment in Figs. 8(b) ($Q_{zz,c}^-$) and 8(c) ($Q_{zz,c}^+$) one can see that this rearrangement of eigenvalues happens at the critical values. Moreover, for $|Q_{zz}^\pm| \ll |Q_{zz,c}^\pm|$ eigenenergies are almost equal for oblate and prolate configurations, as the corresponding wave functions are hardly sensitive to details of the potential.

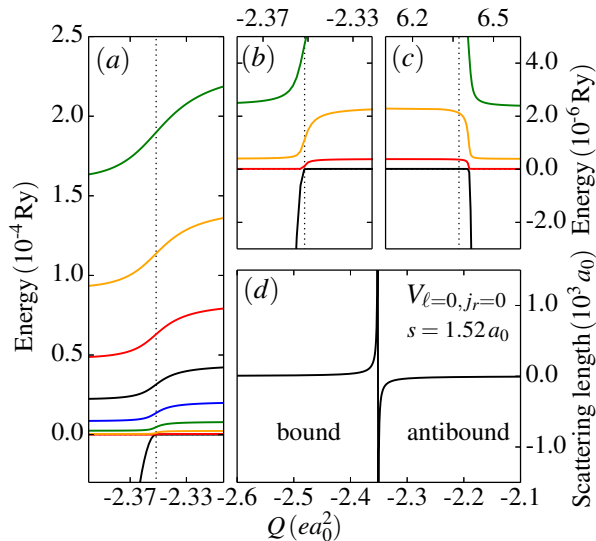


FIG. 8. The low-lying $J^\pi = 0^+$ eigenenergies (real parts) of a quadrupolar anion as a function of the electric quadrupole moment in the vicinity of $Q_{zz,c}^-$ (a,b) and $Q_{zz,c}^+$ (c). Panel (d) shows the scattering length of a scattering state at $E = 10^{-12}$ Ry, which is an eigenstate of the diagonal channel-channel coupling potential $V_{c,c}$ with $c = (\ell = 0, j_r = 0)$ for $s = 1.52 a_0$.

Such an eigenvalue rearrangement at the critical quadrupole moment suggests a critical behavior of the system [128]. The details can be understood by looking at the behavior of the g.s. eigenenergy at the threshold [129]. Indeed as shown in Ref. [99], the bound state energy approaches zero according to:

$$E_{\sigma \rightarrow \sigma_c^+} \sim (\sigma - \sigma_c)^\alpha, \quad (10)$$

where $\sigma = Q_{zz}$, $\sigma_c = Q_{zz,c}$, and α is the critical exponent. For a spherical potential with an asymptotic falloff $\propto 1/r^3$, the critical exponent should be two [99, 128]. In the case considered, the quadrupolar potential is not isotropic, but the dominant g.s. channel wave function has $\ell = 0$.

A fit of the bound-state energy for the oblate configuration, in the range of $Q_{zz}^- \in [-2.4, Q_{zz,c}^-]$, yields $Q_{zz,c}^- = -2.35175 ea_0^2$ and $\alpha = 2.00006$, in agreement with analytical results. The transition of a bound state dominated by $\ell = 0$ to a resonance in quadrupolar anions appears to be a second-order transition [130], which is un-

derstood as a continuous change of the system. This means that there is no bound state at the threshold [99]. The shift of all resonance energies at the critical quadrupole moment is a consequence of this transition, with the bound state changing continuously to reach the energy of the first resonance state. This results in an avoided crossing between the g.s. and the first excited state, which then propagates to all excited states. Avoided crossings in the eigenvalue spectrum of the Hamiltonian reveal the existence of exceptional points [131–133] in its complex extension.

The criticality can also be assessed by considering the scattering length a of the system at different values of Q_{zz} . At low-energy ($k \rightarrow 0$), the scattering length is related to the $\ell = 0$ phase shift $\delta_0(k)$ of a scattering state through:

$$\lim_{k \rightarrow 0} \frac{k}{\tan \delta(k)} = -\frac{1}{a_0}. \quad (11)$$

In our calculations, all partial waves are included up to a given orbital angular momentum cutoff ℓ_{\max} , and even if the $\ell = 0$ component dominates at low energy, there still exist small contributions coming from higher partial waves. In order to illustrate the criticality of the system in a simple case, only the $\ell = 0$ diagonal element of the channel-channel coupling potential has been considered. Indeed, the scaled parameter $q_{s,c} = qs$ reaches a constant [106] at the critical value. Therefore, by changing $s \rightarrow s'$ so that the $\ell = 0$ diagonal element of the potential becomes more and more important, one can effectively evolve the negative critical quadrupole moment $Q_{zz,c,0}^- = -2q_{s',c}s'$ for $\ell = 0$ to the value $Q_{zz,c}^-$ of the complete problem. To this end, one has to decrease s , or conversely increase $q_{s,c}$, to localize the electron in a (almost) pure $\ell = 0$ bound state.

In practice, by considering only $\ell = 0$ wave, one obtains $s = 1.52 a_0$ instead of $1.6 a_0$ for the full problem. The scattering length is plotted as a function of $Q_{zz,c,0}^-$ in Fig. 8(d), and shows a characteristic divergence at the critical value. Such behavior corresponds to the formation of the Feshbach resonance. In the pure $\ell = 0$ case, the negative scattering length is associated with a virtual state, but in the full problem higher partial waves prevent formation of a resonance as shown in Fig. 8(b). This observation on a transition of a bound state into the continuum, together with the divergence of the scattering length, are general features of open quantum systems.

IV. CONCLUSION

In this work, we studied bound and unbound states in quadrupolar anions in a nonadiabatic molecule-plus-electron picture. The Schrödinger equation of the system, expressed in a coupled-channel form, was solved by a diagonalization in the Berggren basis or by means of a direct integration. The BEM and the DIM approaches have been benchmarked against analytical results for the critical electric quadrupole moment. It is shown that binding

energies and r.m.s. radii of bound states in oblate and prolate configurations of a quadrupolar anion follow the two-body halo scaling properties over several orders of magnitude. Using the density of the attached electron in the molecular frame, as well as the collapse of g.s. eigenenergies to the bandhead energy in the adiabatic limit, we demonstrated the existence of regular rotational bands below and above the detachment threshold. The presence of the strong coupling of electron's motion to the molecular core above the threshold makes the situation in quadrupolar anions different from that in dipolar anions, where electron's motion in a resonance state becomes largely decoupled from molecular rotation [80].

We demonstrated the presence of families of narrow resonances close to the rotational states of the molecule. The unbound spectrum contains many quasi-degenerate states, forming regular rotational bands. The presence of narrow resonances close to the threshold, even for subcritical values of Q_{zz} , may produce a low-energy peak in the cross section. Finally, the evolution of a bound state

into the continuum can be described in terms of a second order transition with the critical exponent $\alpha = 2$.

In summary, this work shows that quadrupolar anions are spectacular realizations of open quantum systems. They exhibit fascinating behavior around the detachment threshold, such as halo structures, overlapping resonances, Feshbach resonances, and critical behavior. Consequently, these simple polar molecules constitute an ideal laboratory of weakly bound and unbound quantum states.

ACKNOWLEDGMENTS

This material is based upon work supported by the U.S. Department of Energy, Office of Science, Office of Nuclear Physics under award numbers de-sc0013365 (Michigan State University) and DE-FG02-10ER41700 (French-U.S. Theory Institute for Physics with Exotic Nuclei).

-
- [1] C. Desfrancois, H. Abdoul-Carime, and J. P. Schermann, *Int. J. Mol. Phys. B* **10**, 1339 (1996).
 - [2] R. N. Compton and N. I. Hammer, *Multipole-Bound Molecular Anions*, 1st ed. (Elsevier, 2001).
 - [3] K. D. Jordan and F. Wang, *Annu. Rev. Phys. Chem.* **54**, 367 (2003).
 - [4] J. Simons, *J. Phys. Chem. A* **112**, 6401 (2008).
 - [5] K. Riisager, A. S. Jensen, and P. Møller, *Nucl. Phys. A* **548**, 393 (1992).
 - [6] A. S. Jensen, K. Riisager, D. V. Fedorov, and E. Garrido, *Rev. Mod. Phys.* **76**, 215 (2004).
 - [7] J. Mitroy, *Phys. Rev. Lett.* **94**, 033402 (2005).
 - [8] S. Knoop, F. Ferlino, M. Mark, M. Berninger, H. Schöbel, H. C. Nägerl, and R. Grimm, *Nature Phys.* **5**, 227 (2009).
 - [9] H. W. Hammer and L. Platter, *Annu. Rev. Nucl. Part. Sci.* **60**, 207 (2010).
 - [10] F. Ferlino and R. Grimm, *Physics* **3**, 9 (2010).
 - [11] L. T. T. Frederico, A. Delfino and M. T. Yamashita, *Prog. Part. Nucl. Phys.* **67**, 939 (2012).
 - [12] P. Stipanović, L. V. Markić, I. Bešlić, and J. Boronat, *Phys. Rev. Lett.* **113**, 253401 (2014).
 - [13] M. R. Zirnbauer, J. J. M. Verbaarschot, and H. A. Weidenmüller, *Nucl. Phys. A* **411**, 161 (1983).
 - [14] J. Okołowicz and M. Płoszajczak, *Phys. Rev. C* **80**, 034619 (2009).
 - [15] N. Auerbach and V. Zelevinsky, *Rep. Prog. Phys.* **74**, 106301 (2011).
 - [16] W. von Oertzen, M. Freer, and Y. Kanada-En'yo, *Phys. Rep.* **432**, 43 (2006).
 - [17] M. Freer, *Rep. Prog. Phys.* **70**, 2149 (2007).
 - [18] J. Okołowicz, W. Nazarewicz, and M. Płoszajczak, *Fortschr. Phys.* **61**, 66 (2013).
 - [19] J. Okołowicz, M. Płoszajczak, and W. Nazarewicz, *Prog. Theor. Phys. Supp.* **196**, 230 (2012).
 - [20] P. Kleinwächter and I. Rotter, *Phys. Rev. C* **32**, 1742 (1985).
 - [21] C. Desfrancois, *Phys. Rev. A* **51**, 3667 (1995).
 - [22] H. Abdoul-Carime and C. Desfrancois, *Eur. Phys. J. D* **2**, 149 (1998).
 - [23] H. Abdoul-Carime, J. P. Schermann, and C. Desfrancois, *Few-Body Systems* **31**, 183 (2002).
 - [24] W. R. Garrett, *Chem. Phys. Lett.* **5**, 393 (1970).
 - [25] W. R. Garrett, *J. Chem. Phys.* **71**, 651 (1979).
 - [26] W. R. Garrett, *J. Chem. Phys.* **77**, 3666 (1982).
 - [27] S. Ard, W. R. Garrett, R. N. Compton, L. Adamowicz, and S. G. Stepanian, *Chem. Phys. Lett.* **473**, 223 (2009).
 - [28] K. Fosse, N. Michel, W. Nazarewicz, and M. Płoszajczak, *Phys. Rev. A* **87**, 042515 (2013).
 - [29] K. D. Jordan, *J. Chem. Phys.* **66**, 3305 (1977).
 - [30] G. L. Gutsev, M. Nooijen, and R. J. Bartlett, *Phys. Rev. A* **57**, 1646 (1998).
 - [31] L. Adamowicz, *J. Chem. Phys.* **91**, 7787 (1989).
 - [32] J. S. D. M. A. Smith and L. Adamowicz, *J. Chem. Phys.* **110**, 3804 (1999).
 - [33] D. C. Clary and D. M. Benoit, *J. Chem. Phys.* **111**, 10559 (1999).
 - [34] J. Kalcher and A. F. Sax, *Chem. Phys. Lett.* **326**, 80 (2000).
 - [35] P. Skurski, I. Dąbkowska, A. Sawicka, and J. Rak, *Chem. Phys.* **279**, 101 (2002).
 - [36] K. A. Peterson and M. Gutowski, *J. Chem. Phys.* **116**, 3297 (2002).
 - [37] L. D. Landau and E. M. Lifshitz, *Quantum Mechanics. Non-relativistic Theory*, 1st ed. (Pergamon press, Vol. 3, 1977).
 - [38] H. E. Camblong, L. N. Epele, H. Fanchiotti, and C. A. G. Canal, *Phys. Rev. Lett.* **87**, 220402 (2001).
 - [39] S. A. Coon and B. R. Holstein, *Am. J. Phys.* **70**, 513 (2002).
 - [40] M. Bawin, *Phys. Rev. A* **70**, 022505 (2004).
 - [41] M. Bawin, S. A. Coon, and B. R. Holstein, *Int. J. Mod. Phys. A* **22**, 4901 (2007).
 - [42] J. E. Turner, *Am. J. Phys.* **45**, 758 (1977).
 - [43] E. Fermi and E. Teller, *Phys. Rev.* **72**, 399 (1947).
 - [44] J. M. Lévy-Leblond, *Phys. Rev.* **153**, 1 (1967).

- [45] K. R. Lykke, R. D. Mead, and W. C. Lineberger, *Phys. Rev. Lett.* **52**, 2221 (1984).
- [46] J. Marks, J. I. Brauman, R. D. Mead, K. R. Lykke, and W. C. Lineberger, *J. Chem. Phys.* **88**, 6785 (1988).
- [47] T. Andersen, *Physica Scripta* **T34**, 23 (1991).
- [48] E. A. Brinkman, S. Berger, J. Marks, and J. I. Brauman, *J. Chem. Phys.* **99**, 7586 (1993).
- [49] A. S. Mullin, K. K. Murray, C. P. Schulz, and W. C. Lineberger, *J. Phys. Chem.* **97**, 10281 (1993).
- [50] W. R. Garrett, *Phys. Rev. A* **3**, 961 (1971).
- [51] O. H. Crawford, *Mol. Phys.* **20**, 585 (1971).
- [52] W. R. Garrett, *J. Chem. Phys.* **73**, 5721 (1980).
- [53] W. R. Garrett, *Phys. Rev. A* **22**, 1769 (1980).
- [54] W. R. Garrett, *Phys. Rev. A* **23**, 1737 (1981).
- [55] D. C. Clary, *J. Phys. Chem.* **92**, 3173 (1988).
- [56] D. R. Herrick and P. C. Engelking, *Phys. Rev. A* **29**, 2421 (1984).
- [57] D. C. Clary, *Phys. Rev. A* **40**, 4392 (1989).
- [58] W. R. Garrett, *J. Chem. Phys.* **133**, 224103 (2010).
- [59] H. Estrada and W. Domcke, *J. Phys. B: At. Mol. Phys.* **17**, 279 (1984).
- [60] C. W. Clark, *Phys. Rev. A* **30**, 750 (1984).
- [61] I. I. Fabrikant, *J. Phys. B: At. Mol. Phys.* **18**, 1873 (1985).
- [62] M. McCartney, P. G. Burke, L. A. Morgan, and C. J. Gillan, *J. Phys. B: At. Mol. Opt. Phys.* **23**, L415 (1990).
- [63] J. Martorell, J. G. Muga, and D. W. L. Sprung, *Phys. Rev. A* **77**, 042719 (2008).
- [64] C. A. Nicolaides and E. Brändas, *Unstable States in the Continuous Spectrum. Part I. Analysis, Concepts, Methods and Results*, 1st ed. (Academic Press, 2010).
- [65] C. A. Nicolaides, E. Brändas, and J. R. Sabin, *Unstable States in the Continuous Spectrum. Part II. Interpretation, Theory and Applications*, 1st ed. (Academic Press, 2012).
- [66] M. A. J. S. T. Edwards and J. C. Tully, *J. Chem. Phys.* **136**, 154305 (2012).
- [67] S. F. Wong and G. J. Schulz, *Phys. Rev. Lett.* **33**, 134 (1974).
- [68] K. Rohr and F. Linder, *J. Phys. B: Atom. Molec. Phys.* **8**, L200 (1975).
- [69] K. Rohr and F. Linder, *J. Phys. B: Atom. Molec. Phys.* **9**, 2521 (1976).
- [70] K. Rohr, *J. Phys. B: Atom. Molec. Phys.* **11**, 1849 (1978).
- [71] J. P. Ziesel, G. J. Schulz, and J. Milhaud, *J. Chem. Phys.* **62**, 1936 (1975).
- [72] E. P. Wigner, *Phys. Rev.* **73**, 1002 (1948).
- [73] A. I. Baz', *Sov. Phys. JETP* **6**, 709 (1958).
- [74] A. I. Baz', *Sov. Phys. JETP* **13**, 1058 (1961).
- [75] T. F. O'Malley, *Phys. Rev.* **137**, A1668 (1965).
- [76] H. R. Sadeghpour, J. L. Bohn, M. J. Cavagnero, B. D. Esry, I. I. Fabrikant, J. H. Macek, and A. R. P. Rau, *J. Phys. B: At. Mol. Opt. Phys.* **33**, R93 (2000).
- [77] V. E. Chernov, A. V. Dolgikh, and B. A. Zon, *Phys. Rev. A* **72**, 052701 (2005).
- [78] M. J. Seaton, *Proc. Phys. Soc.* **77**, 174 (1961).
- [79] M. Gaïlitis and R. Damburg, *Sov. Phys. JETP* **17**, 1107 (1963).
- [80] K. Fossez, N. Michel, W. Nazarewicz, M. Płoszajczak, and Y. Jaganathen, *Phys. Rev. A* **91**, 012503 (2015).
- [81] T. Klahn and P. Krebs, *J. Chem. Phys.* **109**, 531 (1998).
- [82] K. D. Jordan and J. F. Liebman, *Chem. Phys. Lett.* **62**, 143 (1979).
- [83] C. Desfrancois, Y. Bouteiller, J. P. Schermann, D. Radisic, S. T. Stokes, K. H. Bowen, N. I. Hammer, and R. N. Compton, *Phys. Rev. Lett.* **92**, 083003 (2004).
- [84] M. Gutowski, P. Skurski, X. Li, and L.-S. Wang, *Phys. Rev. Lett.* **85**, 3145 (2000).
- [85] T. Sommerfeld, *J. Chem. Phys.* **121**, 4097 (2004).
- [86] T. Sommerfeld, K. M. Dreux, and R. Joshi, *J. Phys. Chem. A* **118**, 7320 (2014).
- [87] C. Desfrancois, V. Périquet, S. Carles, J. P. Schermann, and L. Adamowicz, *Chem. Phys.* **239**, 475 (1998).
- [88] G. L. Gutsev and P. Jena, *J. Chem. Phys.* **111**, 504 (1999).
- [89] G. L. Gutsev, R. J. Bartlett, and R. N. Compton, *J. Chem. Phys.* **108**, 6756 (1998).
- [90] M. Gutowski and P. Skurski, *Chem. Phys. Lett.* **303**, 65 (1999).
- [91] M. Allan, *J. Phys. B: At. Mol. Opt. Phys.* **36**, 2489 (2003).
- [92] A. Kalamarides, C. W. Walter, K. A. Smith, and F. B. Dunning, *J. Chem. Phys.* **89**, 7226 (1988).
- [93] K. Harth, M. W. Ruf, and H. Hotop, *Z. Phys. D* **14**, 149 (1989).
- [94] H. S. C. Jr., C. E. Klots, and R. N. Compton, *J. Chem. Phys.* **92**, 5751 (1990).
- [95] S. Barsotti, E. Leber, M. W. Ruf, and H. Hotop, *Int. J. Mass Spectrosc.* **220**, 313 (2002).
- [96] L. Suess, R. Parthasarathy, and F. B. Dunning, *Chem. Phys. Lett.* **372**, 692 (2003).
- [97] R. N. Compton, F. B. Dunning, and P. Nordlander, *Chem. Phys. Lett.* **253**, 8 (1996).
- [98] J. M. Oakes and G. B. Ellison, *Tetrahedron* **42**, 6263 (1986).
- [99] M. Klaus and B. Simon, *Ann. Phys.* **130**, 251 (1980).
- [100] W. C. Wang and L. C. Lee, *J. Chem. Phys.* **84**, 2675 (1986).
- [101] A. Benz, O. Leisin, H. Morgner, H. Seiberle, and J. Stegmaier, *Z. Phys. A* **320**, 11 (1985).
- [102] R. A. Popple, C. D. Finch, and F. B. Dunning, *Chem. Phys. Lett.* **234**, 172 (1995).
- [103] M. V. N. A. Prasad and R. F. Wallis, *Phys. Rev. B* **40**, 5924 (1989).
- [104] M. V. N. A. Prasad and R. F. Wallis, *Solid State Commun.* **77**, 973 (1991).
- [105] A. D. Buckingham, *Q. Rev. Chem. Soc.* **13**, 183 (1959).
- [106] A. Ferron, P. Serra, and S. Kais, *J. Chem. Phys.* **120**, 18 (2004).
- [107] V. Privman, *Finite Size Scaling and Numerical Simulation of Statistical Systems*, 1st ed. (World Scientific, 1990).
- [108] J. P. Neirotti, P. Serra, and S. Kais, *Phys. Rev. Lett.* **79**, 3142 (1997).
- [109] P. Serra, J. P. Neirotti, and S. Kais, *Phys. Rev. A* **57**, R1481(R) (1998).
- [110] S. Kais and P. Serra, *Int. Rev. Phys. Chem.* **19**, 97 (2000).
- [111] V. I. Pupyshev and A. Y. Ermilov, *Int. J. Quant. Chem.* **96**, 185 (2004).
- [112] C. A. Bertulani, H. W. Hammer, and U. van Kolck, *Nucl. Phys. A* **712**, 37 (2002).
- [113] P. F. Bedaque, H. W. Hammer, and U. V. Kolck, *Phys. Lett. B* **569**, 159 (2003).
- [114] A. Bohr and B. R. Mottelson, *Nuclear Structure, Vol. 2: Nuclear Deformations*, 1st ed. (World Scientific, Singapore, 1998).

- [115] W. R. Garrett, *J. Chem. Phys.* **128**, 194309 (2008).
- [116] T. Berggren, *Nucl. Phys. A* **109**, 265 (1968).
- [117] N. Michel, W. Nazarewicz, M. Płoszajczak, and T. Vertse, *J. Phys. G: Nucl. Part. Phys.* **36**, 013101 (2009).
- [118] R. G. Newton, *Scattering Theory of Waves and Particles*, 2nd ed. (Springer-Verlag, New York, 1982).
- [119] A. M. Dykhne and A. V. Chaplik, *Sov. Phys. JETP* **13**, 1002 (1961).
- [120] B. Gyarmati and T. Vertse, *Nucl. Phys. A* **160**, 523 (1971).
- [121] B. Simon, *Phys. Lett. A* **71**, 211 (1979).
- [122] N. Michel, W. Nazarewicz, M. Płoszajczak, and K. Benhaceur, *Phys. Rev. Lett.* **89**, 042502 (2002).
- [123] N. Michel, W. Nazarewicz, M. Płoszajczak, and J. Okołowicz, *Phys. Rev. C* **67**, 054311 (2003).
- [124] *NIST Chemistry WebBook* (The National Institute of Standards and Technology, 2016).
- [125] W. R. Garrett, *J. Chem. Phys.* **136**, 054116 (2012).
- [126] T. Misu, W. Nazarewicz, and S. Åberg, *Nucl. Phys. A* **614**, 44 (1997).
- [127] S.-G. Zhou, J. Meng, P. Ring, and E.-G. Zhao, *Phys. Rev. C* **82**, 011301 (2010).
- [128] M. Lassaut, I. Bulboaca, and R. J. Lombard, *J. Phys. A: Math. Gen.* **29**, 2175 (1996).
- [129] N. Moiseyev, *Phys. Rep.* **302**, 212 (1998).
- [130] P. Serra, S. Kais, and N. Moiseyev, *Phys. Rev. A* **64**, 062502 (2001).
- [131] J. Okołowicz, M. Płoszajczak, and I. Rotter, *Phys. Rep.* **374**, 271 (2003).
- [132] E. Hernández, A. Jáuregui, and A. Mondragón, *Phys. Rev. E* **84**, 046209 (2011).
- [133] W. D. Heiss, *J. Phys. A: Math. Theor.* **45**, 444016 (2012).